TU Delft

Delft University of Technology

Document Version
Final published version

Licence
CC BY

Citation (APA)
Plokker, M. P., Bergkamp, S. W., & Hintzen, H. T. (2026). Evidence for Tm2+→Tm3+ energy transfer in Tm-doped BaCl2 for potential use in opto-electronic devices. *Optical Materials: X*, *29*, Article 100432. https://doi.org/10.1016/j.omx.2025.100432

Important note
To cite this publication, please use the final published version (if applicable).
Please check the document version above.

Copyright
In case the licence states “Dutch Copyright Act (Article 25fa)”, this publication was made available Green Open Access via the TU Delft Institutional Repository pursuant to Dutch Copyright Act (Article 25fa, the Taverne amendment). This provision does not affect copyright ownership.
Unless copyright is transferred by contract or statute, it remains with the copyright holder.

Sharing and reuse
Other than for strictly personal use, it is not permitted to download, forward or distribute the text or part of it, without the consent of the author(s) and/or copyright holder(s), unless the work is under an open content license such as Creative Commons.

Takedown policy
Please contact us and provide details if you believe this document breaches copyrights.
We will remove access to the work immediately and investigate your claim.

This work is downloaded from Delft University of Technology.

Optical Materials: X 29 (2026) 100432

Contents lists available at ScienceDirect

Optical Materials: X

journal homepage: www.journals.elsevier.com/optical-materials-x

Evidence for Tm^{2+}→Tm^{3+} energy transfer in Tm-doped $BaCl_2$ for potential use in opto-electronic devices

M.P. Plokker [a,b,*], S.W. Bergkamp [a], H.T. Hintzen [a]

[a] Luminescence Materials Research Group, Delft University of Technology, Mekelweg 15, 2629 JB, Delft, the Netherlands
[b] Rheinisch-Westfälisches Elektrizitätswerk, RWE Generation NL, Amerweg 1, 4931 NC, Geertruidenberg, the Netherlands

A B S T R A C T

The energy transfer from Tm^{2+} to Tm^{3+}, which has not yet been reported before, has now been observed for the first time. It was found that orthorhombic $BaCl_2$:Tm^{2+},Tm^{3+} with the $PbCl_2$ cotunnite structure shows the luminescence properties to enable Tm^{2+}→Tm^{3+} energy transfer. Evaluation of the luminescence properties of $BaCl_2$:Tm^{2+},Tm^{3+} in detail and other Tm^{2+}/Tm^{3+}-activated phosphors in general makes clear that the conditions for Tm^{2+}→Tm^{3+} energy transfer are a strong overlap of the Tm^{2+} spin-allowed $4f^{12}5d^1$→$4f^{13}$ emission with Tm^{3+} $^3H_6$→$^3F_3$ or $^3H_6$→$^3H_4$ ($4f^{12}$→$4f^{12}$) excitations or overlap of the Tm^{2+} spin-forbidden $4f^{12}5d^1$→$4f^{13}$ emission with Tm^{3+} $^3H_6$→$^3H_4$ ($4f^{12}$→$4f^{12}$) excitation, resulting in both cases in interconfigurational transitions, while the Tm^{2+} spin-allowed $4f^{12}5d^1$→$4f^{13}$ emission should not overlap with the Tm^{2+} spin-forbidden $4f^{13}$→$4f^{12}5d^1$ excitation. In addition, the Tm^{2+}-Tm^{3+} distance has to be small, preferably for a high Tm^{2+} concentration to increase the absorption of excitation radiation in combination with a low Tm^{3+} concentration in order to avoid concentration quenching of the luminescence. Finally, implications of Tm^{2+}→Tm^{3+} energy transfer for applications such as luminescent solar concentrators are discussed.

1. Introduction

Lanthanide-doped materials are well known because of their special luminescence properties which are used in applications such as e.g. LED, afterglow, scintillation, anti-counterfeiting and thermometric phosphors. All lanthanide ions are stable in the trivalent state, while many of them also occur in the divalent state, such as Eu, Yb, Sm, Tm, Dy and Nd [1].

Eu is the metal of which the trivalent state can be most easily reduced to the divalent state [2]. Both Eu valencies are well known for application in commercial phosphors, e.g. Y_2O_3:Eu^{3+} and $BaMgAl_{10}O_{17}$:Eu^{2+} (traditional TL fluorescent lamps phosphors) Gd_2O_3:Eu^{3+} (scintillation phosphor), Sr_2SiO_4:Eu^{2+}, β-Sialon:Eu^{2+} and $(Ca,Sr,Ba)_2Si_5N_8$:Eu^{2+} (LED conversion phosphors). Coexistence of Eu^{2+} and Eu^{3+} in a single host lattice may result in beneficial effects (Eu^{2+} can act as a sensitiser of Eu^{3+} luminescence [3,4]) or detrimental effects (Eu^{3+} can act as a killer centre for Eu^{2+} luminescence [5,6]). Sensitization of Eu^{3+} luminescence by energy transfer from Eu^{2+} to Eu^{3+} has been demonstrated for several mixed valency Eu-doped phosphors, such as YF_3:Eu^{2+},Eu^{3+} [7] and $CaAl_2Si_2O_8$:Eu^{2+},Eu^{3+} [8]. A white light emitting phosphor can be realized by combining the characteristic red Eu^{3+} emission with blue-green Eu^{2+} emission (at 490–500 nm) in a single host lattice, as has been shown for e.g. $MgSrLa_8(SiO_4)_6O_2$:Eu^{2+},Eu^{3+} [9] and $Na_5Al(PO_4)_2F_2$:Eu^{2+},Eu^{3+} [10]. Recently the change of the characteristics of Eu^{2+} versus Eu^{3+} emissions (such as Eu^{2+}/Eu^{3+} intensity ratio), as a function of temperature, attracts attention for the design of thermosensitive phosphors for application in the field of remote temperature sensing [11].

After Eu, Yb gets most easily reduced, followed by Sm and then Tm [2]. Energy transfer from Ln^{2+} to Ln^{3+} has also been found for Ln = Yb [12] and Ln = Sm [13], but has not yet been reported for Ln = Tm. Tm reduction is much more difficult and special conditions are required to convert Tm^{3+} into Tm^{2+}. Therefore Tm^{2+}-doped materials are normally contaminated with some smaller or larger amount of Tm^{3+} if starting with Tm^{3+} raw materials. This can influence the luminescence of Tm^{2+}-doped phosphors which are investigated because of promising properties for maser [14–17] and upconversion [18–25] applications, luminescent solar concentrators [26–30], luminescent thermometers [31–36], etc. An example is Tm-doped $BaCl_2$, with the orthorhombic cotunnite structure, in which Tm^{2+} and Tm^{3+} do coexist, and which was recently studied by us with respect to quenching dynamics [37] and thermal quenching behaviour [38]. In this follow-up research on $BaCl_2$:Tm^{2+},Tm^{3+} we report for the first time the energy transfer from Tm^{2+} to Tm^{3+} and in addition discuss the implications for the luminescence characteristics and potential applications.

* Corresponding author. Luminescence Materials Research Group, Delft University of Technology, Mekelweg 15, 2629 JB, Delft, the Netherlands.
E-mail address: maartenplokker@hotmail.com (M.P. Plokker).

https://doi.org/10.1016/j.omx.2025.100432
Received 29 October 2025; Received in revised form 30 November 2025; Accepted 6 December 2025
Available online 14 January 2026
2590-1478/© 2026 The Author(s). Published by Elsevier B.V. This is an open access article under the CC BY license (http://creativecommons.org/licenses/by/4.0/).

2. Experimental section

2.1. Sample synthesis and characterisation

The synthesis conditions for the $BaCl_2$:Tm^{2+},Tm^{3+} sample are described in our recent work on the Tm^{2+} relaxation dynamics in orthorhombic $BaCl_2$ [37], whereas those of the $BaCl_2$:Tm^{3+} sample are provided in our article on the relative positioning of the Tm^{2+} energy levels versus the $BaCl_2$ bandgap [38]. As described in these works, X-Ray Diffraction (XRD) measurements (Philips X'pert-Pro, Eindhoven, The Netherlands), with sealed sample holders, revealed that both samples exhibit the orthorhombic cotunnite $PbCl_2$ structure with space group *Pnma* (No. 62). This implies that the Tm^{2+} and/or Tm^{3+} ions that occupy the Ba^{2+}-site have C_S point group site symmetry, combined with a 9-fold anion coordination geometry [39]. Furthermore, ICP-OES measurements (PerkinElmer Optima 4300DV, Waltham Massachusetts, USA) combined with Kubelka-Munk (K-M) absorption spectroscopy measurements (Bruker Vertex V80, Karlsruhe, Germany) previously enabled us [37,38] to determine that the $BaCl_2$:Tm^{2+},Tm^{3+} sample contained around 0.3 mol% Tm^{2+} and 0.8 mol% Tm^{3+}, whereas the $BaCl_2$:Tm^{3+} sample contained 1.5 mol% Tm^{3+}.

2.2. Luminescence measurements

The low temperature excitation and emission spectra were obtained using a Xenon lamp coupled to a double excitation monochromator with three gratings and a R7600U–20HV–800V PMT, H1033A-75 NIR-PMT or C9100-13 EM-CCD (all Hamamatsu Photonics, Hamamatsu, Japan) that was in turn attached to a single emission monochromator with three gratings. A calibrated EPLAB NBS 1000W Quartz Iodine lamp was used to acquire the wavelength dependent sensitivity of the detectors. In addition, the samples were heated and cooled by an APD Cryogenic Helium cooler (APD Cryogenics, Allentown Pennsylvania, USA) and Lakeshore temperature controller (Lakeshore Cryotronics, Westerville Ohio, USA). Special hygroscopic sampleholders were used during all measurements to prevent unwanted hydrolysis and oxidation reactions [40].

3. Results and discussion

3.1. Tm^{2+} and Tm^{3+} Energy levels and luminescence

For the $BaCl_2$:Tm^{2+},Tm^{3+} sample, the top panel in Fig. 1 shows the Tm^{2+} excitation spectrum (dark blue) as acquired on the $^2F_{5/2} \rightarrow {}^2F_{7/2}$ ($4f^{13} \rightarrow 4f^{13}$) emission at 20 K. Various Tm^{2+} $4f^{12}5d^1$ excitation bands can be observed. Due to the small Tm^{2+} $4f^{12}5d^1$ crystal field splitting, as a consequence of the large and asymmetric Ba^{2+}-site, the excitation bands are closely spaced in energy, making it difficult to separate between them. In our previous work on orthorhombic $BaCl_2$:Tm^{2+} [37], we were therefore only able to identify the lowest energy Tm^{2+} $4f^{12}5d^1$

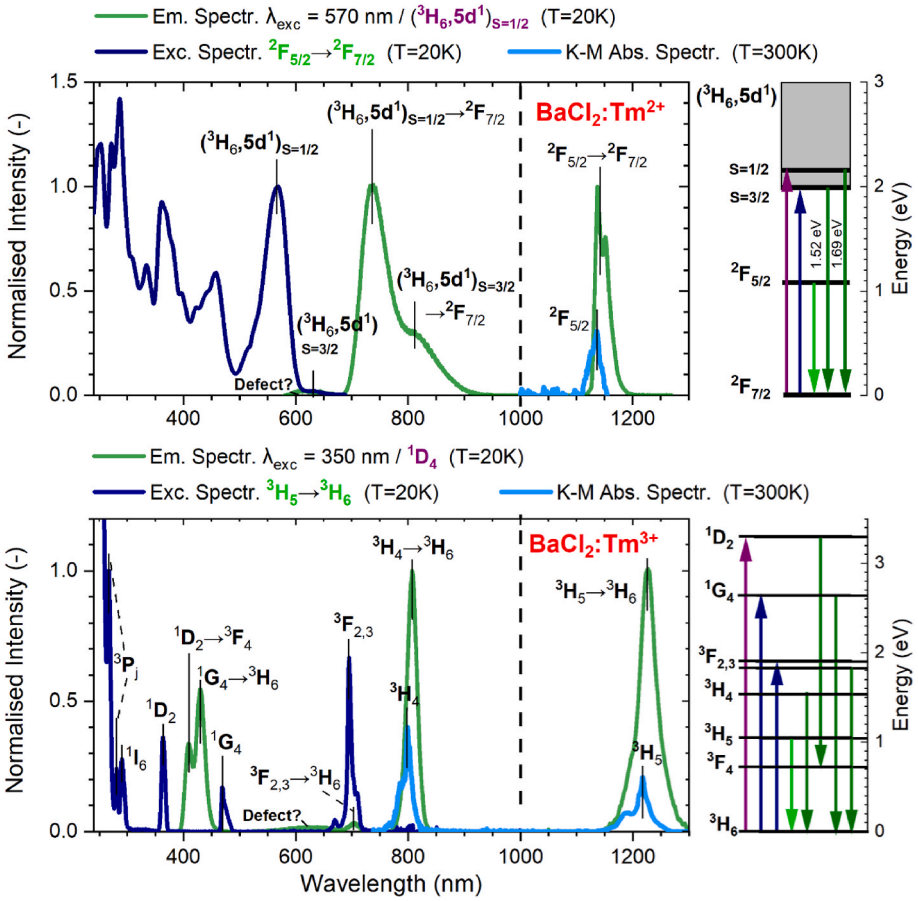

Fig. 1. Top – $BaCl_2$:Tm^{2+},Tm^{3+} sample: Room-temperature KM absorption spectrum (light blue), the 20 K excitation spectrum as acquired on the Tm^{2+} $^2F_{5/2} \rightarrow {}^2F_{7/2}$ emission (dark blue), and the 20 K emission spectrum after photoexcitation at 570 nm into the Tm^{2+} $(^3H_6,5\ d^1)_{S\ =\ 1/2}$ levels (green). The herein observed Tm^{2+} excitation levels and Tm^{2+} emissions have been labelled in accordance to our previous work [37] with a scaled levels scheme provided to the right.
Bottom – $BaCl_2$:Tm^{3+} sample: Room-temperature KM absorption spectrum (light blue), the 20 K excitation spectrum as acquired on the Tm^{3+} $^3H_5 \rightarrow {}^3H_6$ emission (dark blue), and the 20 K emission spectrum after photoexcitation at 360 nm into the Tm^{3+} $^1D_2$ level (green). The herein observed Tm^{3+} excitation levels and Tm^{3+} emissions have been labelled in accordance to the work of Carnall et al. [41] and our previous work on $BaCl_2$:Tm^{3+} [38], with a scaled levels scheme provided to the right.

excitation levels. As such, the broad excitation band at around 570 nm was found to represent the $(^3H_6,5\ d^1)_{S\ =\ 1/2}$ levels, whereas the weak band positioned at about 630 nm is connected to the $(^3H_6,5\ d^1)_{S\ =\ 3/2}$ levels. In addition, a small part of the room temperature K-M absorption spectrum (light blue) is added to the figure to reveal the precise location of the Tm^{2+} $^2F_{5/2}$ ($4f^{13}$) absorption level. An overview of the different Tm^{2+} $4f^{12}5d^1$ and $4f^{13}$ levels is provided in the scaled level scheme at the top right of Fig. 1.

After exciting into the Tm^{2+} $(^3H_6,5\ d^1)_{S\ =\ 1/2}$ $4f^{12}5d^1$-levels at 20 K, an emission spectrum was captured (green) in which three distinct Tm^{2+} emissions are observed. These emissions were previously classified and labelled by us in accordance to their transition [37]. The broad emission feature near 815 nm was associated with the spin-forbidden $(^3H_6,5\ d^1)_{S\ =\ 3/2} \rightarrow\ ^2F_{7/2}$ transition, whereas the emission peak at about 735 nm was found to correspond to the spin-allowed $(^3H_6,5\ d^1)_{S\ =\ 1/2} \rightarrow\ ^2F_{7/2}$ transition. Both emissions represent Tm^{2+} $4f^{12}5d^1 \rightarrow 4f^{13}$ emissions. Furthermore, the sharp emission peak near 1140 nm could be related to the $^2F_{5/2} \rightarrow\ ^2F_{7/2}$ transition and represents the Tm^{2+} $4f^{13} \rightarrow 4f^{13}$ line-emission. For convenience, the three Tm^{2+} emissions are appended to the scaled level scheme at the top right of Fig. 1.

For the $BaCl_2$:Tm^{3+} sample, the lower panel in Fig. 1 displays the Tm^{3+} excitation spectrum (dark blue) as obtained on the $^3H_5 \rightarrow\ ^3H_6$ ($4f^{12} \rightarrow 4f^{12}$) emission at 20 K. A great variety of sharp excitation peaks can be perceived, which can be classified with help of the Dieke diagram [42] and the tabulated work of Carnall et al. [41] As such, the excitation peaks at around 700 nm can be coupled to the $^3F_{2,3}$ levels, the peak at 470 nm to the $^1G_4$ level, the peak at 360 nm to the $^1D_2$ level, the peak at 280 nm to the $^1I_6$ level and the peaks at 280 and 265 nm to the ^3P_j levels. Moreover, a part of the room-temperature K-M absorption spectrum (light blue) is added showing the locations of the $^3H_4$ and $^3H_5$ levels at 795 and 1215 nm, respectively. An overview of these observed Tm^{3+} $4f^{12}$ excitation levels is offered by the scaled level scheme at the bottom right of Fig. 1.

Upon exciting into the Tm^{3+} $^1D_2$ $4f^{12}$-level at 20 K, an emission spectrum was recorded (green) that reveals five groups of sharp Tm^{3+} $4f^{12} \rightarrow 4f^{12}$ line-emissions. These five emissions were classified to their transition with help of our previous work on $BaCl_2$:Tm^{3+} [38]. The related transition labels are added to the figure. Accordingly, the emission close by 1225 nm can be connected to the $^3H_5 \rightarrow\ ^3H_6$ transition, the emission near 805 nm can be related to the $^3H_4 \rightarrow\ ^3H_6$ transition, the emission at 705 nm matches the position of the $^3F_{2,3} \rightarrow\ ^3H_6$ transition, the emission at 430 nm is associated with the $^1G_4 \rightarrow\ ^3H_6$ transition and the emission at 410 nm to the $^1D_2 \rightarrow\ ^3F_4$ transition. For convenience, the Tm^{3+} emissions are appended to the scaled level scheme at the bottom right of Fig. 1.

3.1.1. Luminescence feature at 580–675 nm

The emission spectra of both the $BaCl_2$:Tm^{2+},Tm^{3+} and the $BaCl_2$:Tm^{3+} sample display a very weak bump centred near 640 nm. This feature has recently also been observed by Gareev et al. [43] while studying the sonoluminescence of $TmCl_2$ and $TmCl_3$ nanoparticles with a size of 20–35 nm suspended in dodecane. It can therefore not be attributed to an artifact e.g. originating from our sampleholder, as was suggested by us previously [37]. However, Gareev et al. [43] ascribe the emission at about 600 nm to a Tm^{2+} $5d^14f^{12} \rightarrow 4f^{13}$ transition, suggesting that our emission at about 640 nm may be due to Tm^{2+} located in irregular sites at or near the surface.

3.2. $Tm^{2+} \rightarrow Tm^{3+}$ energy transfer in orthorhombic Tm-doped $BaCl_2$

With the Tm^{2+} and Tm^{3+} levels classified and the emissions and excitations labelled in accordance to their transition, it can be perceived that the Tm^{2+} emission spectrum (green) of the $BaCl_2$:Tm^{2+},Tm^{3+} sample and the Tm^{3+} excitation (dark blue) and absorption (light blue) spectrum of the $BaCl_2$:Tm^{3+} sample share a spectral overlap in the wavelength range of 680–830 nm. This can also be observed based on the scaled level schemes to the right of Fig. 1. The broad Tm^{2+} $(^3H_6,5\ d^1)_{S\ =\ 1/2} \rightarrow\ ^2F_{7/2}$ and $(^3H_6,5\ d^1)_{S\ =\ 3/2} \rightarrow\ ^2F_{7/2}$ emissions cover an energy range in which also the Tm^{3+} $^3H_6 \rightarrow\ ^3F_{2,3}$ and $^3H_6 \rightarrow\ ^3H_4$ excitation levels are situated. For a mixed valent sample, $BaCl_2$:Tm^{2+},Tm^{3+}, this would make it possible to have energy transfer from Tm^{2+} to Tm^{3+}, with the prerequisite of sufficiently small distances between both ions. In this scenario, Tm^{2+} will act as the sensitiser, whereas the Tm^{3+} will be the activator.

3.2.1. Schematic overview

The anticipated $Tm^{2+} \rightarrow Tm^{3+}$ energy transfer in orthorhombic $BaCl_2$, is indicated in Fig. 2, where photoexcitation at 570 nm will excite the Tm^{2+} $^2F_{7/2}$ ground state to the Tm^{2+} $(^3H_6,5\ d^1)_{S\ =\ 1/2}$ $4f^{12}5d^1$-levels at 2.17 eV or 17545 cm^{-1}. This will trigger Tm^{2+} spin-allowed $(^3H_6,5\ d^1)_{S\ =\ 1/2} \rightarrow\ ^2F_{7/2}$ ($4f^{12}5d^1 \rightarrow 4f^{13}$) luminescence, present within the range of 11445–15365 cm^{-1}, with its peak located at an energy of 13605 cm^{-1} or 1.69 eV. The small energy gap of 1675 cm^{-1}, corresponding with 8 phonons [44], between the Tm^{2+} $(^3H_6,5\ d^1)_{S\ =\ 1/2}$ and $(^3H_6,5\ d^1)_{S\ =\ 3/2}$ $4f^{12}5d^1$-levels will result in relaxation towards the $(^3H_6,5\ d^1)_{S\ =\ 3/2}$ levels via multiphonon relaxation, inducing spin-forbidden $(^3H_6,5\ d^1)_{S\ =\ 3/2} \rightarrow\ ^2F_{7/2}$ ($4f^{12}5d^1 \rightarrow 4f^{13}$) luminescence over an energy range of 9550–15080 cm^{-1} with its peak centred at 12270 cm^{-1} or 1.52 eV. When a Tm^{3+} ion is in close proximity, energy can be transferred from Tm^{2+} to Tm^{3+} via the Tm^{2+} $(^3H_6,5\ d^1)_{S\ =\ 1/2} \rightarrow\ ^2F_{7/2}$ ($4f^{12}5d^1 \rightarrow 4f^{13}$) transition, exciting the Tm^{3+} ion from the $^3H_6$ ground state to the $^3F_{2,3}$ and $^3H_4$ levels, respectively situated at 15190, 14555 and 12705 cm^{-1}. This will result in the appearance of Tm^{3+} $^3F_{2,3} \rightarrow\ ^3H_6$ and $^3H_4 \rightarrow\ ^3H_6$ ($4f^{12} \rightarrow 4f^{12}$) emissions alongside the aforementioned Tm^{2+} $(^3H_6,5\ d^1)_{S\ =\ 1/2} \rightarrow\ ^2F_{7/2}$ emission. In a much similar fashion, the Tm^{2+} $(^3H_6,5\ d^1)_{S\ =\ 3/2} \rightarrow\ ^2F_{7/2}$ ($4f^{12}5d^1 \rightarrow 4f^{13}$) luminescence will trigger Tm^{3+} $^3F_3 \rightarrow\ ^3H_6$ and $^3H_4 \rightarrow\ ^3H_6$ ($4f^{12} \rightarrow 4f^{12}$) luminescence of respectively around 14185 and 12420 cm^{-1}. Summarizing, Tm^{2+} $^2F_{7/2} \rightarrow (^3H_6,5\ d^1)_{S\ =\ 1/2}$ ($4f^{13} \rightarrow 4f^{12}5d^1$) excitation leads to $Tm^{2+} \rightarrow Tm^{3+}$ energy transfer as evidenced by an observation of the Tm^{3+} $^3F_{2,3} \rightarrow\ ^3H_6$ and $^3H_4 \rightarrow\ ^3H_6$ ($4f^{12} \rightarrow 4f^{12}$) emissions. At low temperatures, the Tm^{3+} $^3F_{2,3} \rightarrow\ ^3H_6$ ($4f^{12} \rightarrow 4f^{12}$) narrow line emissions can be easily discriminated from the broad Tm^{2+} $4f^{12}5d^1 \rightarrow 4f^{12}$ emissions, but as Fig. 1 shows, the Tm^{3+} $^3H_4 \rightarrow\ ^3H_6$ emission overlaps with the Tm^{2+} $(^3H_6,5\ d^1)_{S\ =\ 3/2} \rightarrow\ ^2F_{7/2}$ ($4f^{12}5d^1 \rightarrow 4f^{12}$) emission. A separation would be less complicated at a temperature where the Tm^{2+} luminescence has quenched and is hardly observed anymore in the emission spectra. We have therefore decided to investigate the $Tm^{2+} \rightarrow Tm^{3+}$ energy transfer at room temperature, despite the potentially strong presence of thermal quenching effects, as detailed in section 9.1 in the Supplementary Info (SI) [37,38].

3.2.2. Emission spectra

Fig. 3 shows the normalised room-temperature emission spectrum for both the $BaCl_2$:Tm^{2+},Tm^{3+} and $BaCl_2$:Tm^{3+} samples, after photoexcitation at 570 nm or 17545 cm^{-1} (about 2.2 eV). For the $BaCl_2$:Tm^{2+}, Tm^{3+} sample (red), the photoexcitation energy matches with the required energy for the Tm^{2+} $^2F_{7/2} \rightarrow (^3H_6,5\ d^1)_{S\ =\ 1/2}$ ($4f^{13} \rightarrow 4f^{12}5d^1$) transition, whereas for the $BaCl_2$:Tm^{3+} sample no direct excitations can occur as there are no Tm^{3+} $4f^{13}$-levels located between 21310 ($^1G_4$) and 15190 cm^{-1} ($^3F_2$) [42,41]. As is observed in the emission spectrum of the $BaCl_2$:Tm^{2+},Tm^{3+} sample, weak peaks of the Tm^{2+} $(^3H_6,5\ d^1)_{S\ =\ 1/2} \rightarrow\ ^2F_{7/2}$ and $(^3H_6,5\ d^1)_{S\ =\ 3/2} \rightarrow\ ^2F_{7/2}$ ($4f^{12}5d^1 \rightarrow 4f^{13}$) emissions remain observable near 13700 and 12255 cm^{-1}, respectively. They are located on top or close to the previously discussed luminescence feature near 610 nm. In addition, small but clear signatures of the Tm^{3+} $^3F_2 \rightarrow\ ^3H_6$ and $^3F_3 \rightarrow\ ^3H_6$ ($4f^{12} \rightarrow 4f^{12}$) emissions at about 14515 and 14245 cm^{-1} are respectively observed, and possibly also of the Tm^{3+} $^3H_4 \rightarrow\ ^3H_6$ ($4f^{12} \rightarrow 4f^{12}$) emission which would be hidden in the tail of the Tm^{2+} $(^3H_6,5\ d^1)_{S\ =\ 3/2} \rightarrow\ ^2F_{7/2}$ emission. Moreover, for confirmation, these Tm^{3+} emissions are not observed in the emission spectrum of the $BaCl_2$:Tm^{3+} sample (blue). It provides a strong indication of the anticipated $Tm^{2+} \rightarrow Tm^{3+}$ energy transfer.

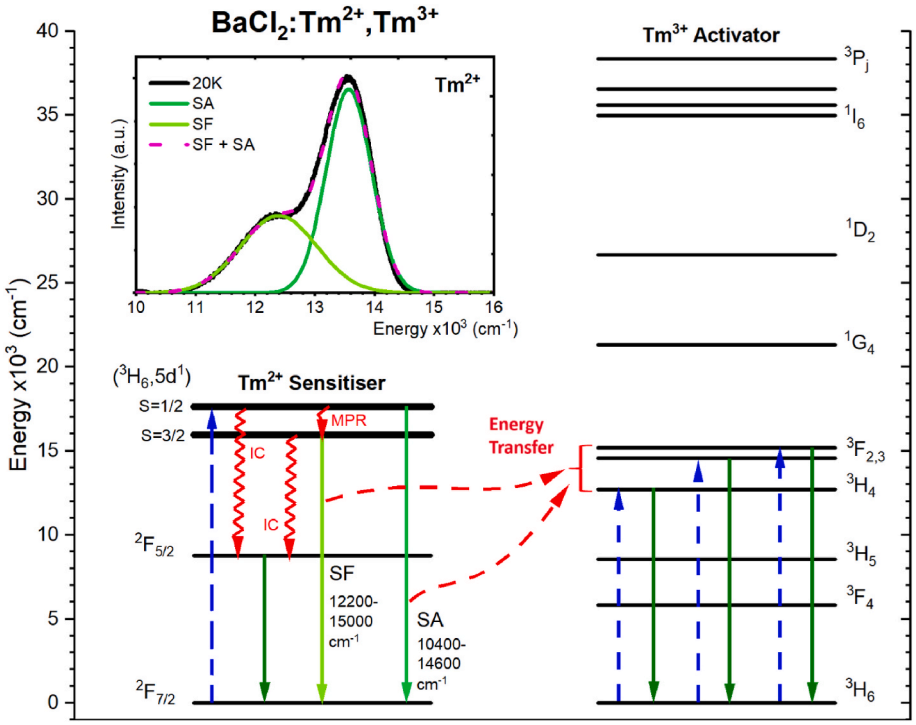

Fig. 2. Diagram illustrating the energy transfer from Tm^{2+} (sensitiser) to Tm^{3+} (activator) in $BaCl_2$:Tm^{2+},Tm^{3+}. Left bottom: upon exciting into the Tm^{2+} $(^3H_6,5\ d^1)_{S\ =\ 1/2}$ levels three emissions are observed at low temperature: the Spin-Allowed $(^3H_6,5\ d^1)_{S\ =\ 1/2} \rightarrow {}^2F_{7/2}$ ($4f^{12}5d^1 \rightarrow 4f^{13}$) emission with energy 11445-15365 cm^{-1}, the Spin-Forbidden $(^3H_6,5\ d^1)_{S\ =\ 3/2} \rightarrow {}^2F_{7/2}$ ($4f^{12}5d^1 \rightarrow 4f^{13}$) emission with energy 9550-15080 cm^{-1} and the ${}^2F_{5/2} \rightarrow {}^2F_{7/2}$ ($4f^{13} \rightarrow 4f^{13}$) emission [36]. At higher temperatures, the two $4f^{12}5d^1 \rightarrow 4f^{13}$ emissions undergo quenching and feed the ${}^2F_{5/2}$ $4f^{13}$-level from which the ${}^2F_{5/2} \rightarrow {}^2F_{7/2}$ emission emerges [36]. Left top: deconvoluted emission spectra of the SA $(^3H_6,5\ d^1)_{S\ =\ 1/2} \rightarrow {}^2F_{7/2}$ and SF $(^3H_6,5\ d^1)_{S\ =\ 3/2} \rightarrow {}^2F_{7/2}$ emissions with energy scale on the x-axis. Right: the energy of the Tm^{2+} $(^3H_6,5\ d^1)_{S\ =\ 1/2} \rightarrow {}^2F_{7/2}$ and SF $(^3H_6,5\ d^1)_{S\ =\ 3/2} \rightarrow {}^2F_{7/2}$ ($4f^{12}5d^1 \rightarrow 4f^{13}$) emissions matches with the excitation energy of the Tm^{3+} ${}^3F_{2,3}$ and ${}^3H_4$ $4f^{12}$-levels at respectively 15190, 14555 and 12705 cm^{-1} [37,38], enabling $Tm^{2+} \rightarrow Tm^{3+}$ energy transfer. This transfer process would result in the observation of Tm^{3+} ${}^3F_{2,3} \rightarrow {}^3H_6$ and ${}^3H_4 \rightarrow {}^3H_6$ luminescence.

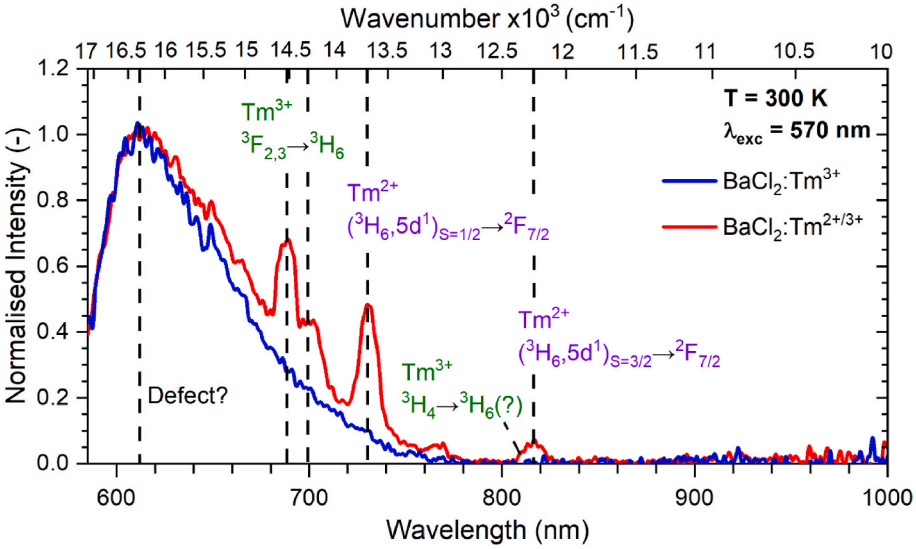

Fig. 3. Normalised room temperature emission spectra for the $BaCl_2$:Tm^{2+},Tm^{3+} sample (red curve) and $BaCl_2$:Tm^{3+} sample (blue curve). After photoexcitation at 570 nm or 17545 cm^{-1}, corresponding to the energy of the Tm^{2+} $(^3H_6,5\ d^1)_{S\ =\ 1/2}$ LS levels, several Tm^{2+} and Tm^{3+} emissions appear in the spectrum of the $BaCl_2$:Tm^{2+},Tm^{3+} sample, as respectively indicated by the violet and green transitions. For the $BaCl_2$:Tm^{3+} sample no Tm^{3+} emissions appear after exciting at 570 nm or 17545 cm^{-1}.

3.2.3. *Excitation spectra*

As a next step, excitation spectra were measured on most of the observed Tm^{3+} and Tm^{2+} emission peaks and compared to the excitation spectrum of the Tm^{2+} ${}^2F_{5/2} \rightarrow {}^2F_{7/2}$ ($4f^{13} \rightarrow 4f^{13}$) emission. These spectra were all acquired with the $BaCl_2$:Tm^{2+},Tm^{3+} sample and are presented in Fig. 4. As this figure shows, the excitation spectra related to the Tm^{2+} ${}^2F_{5/2} \rightarrow {}^2F_{7/2}$ (purple) and $(^3H_6,5\ d^1)_{S\ =\ 1/2} \rightarrow {}^2F_{7/2}$ (red) ($4f^{12}5d^1 \rightarrow 4f^{13}$) emissions show much resemblance (apart from a slight

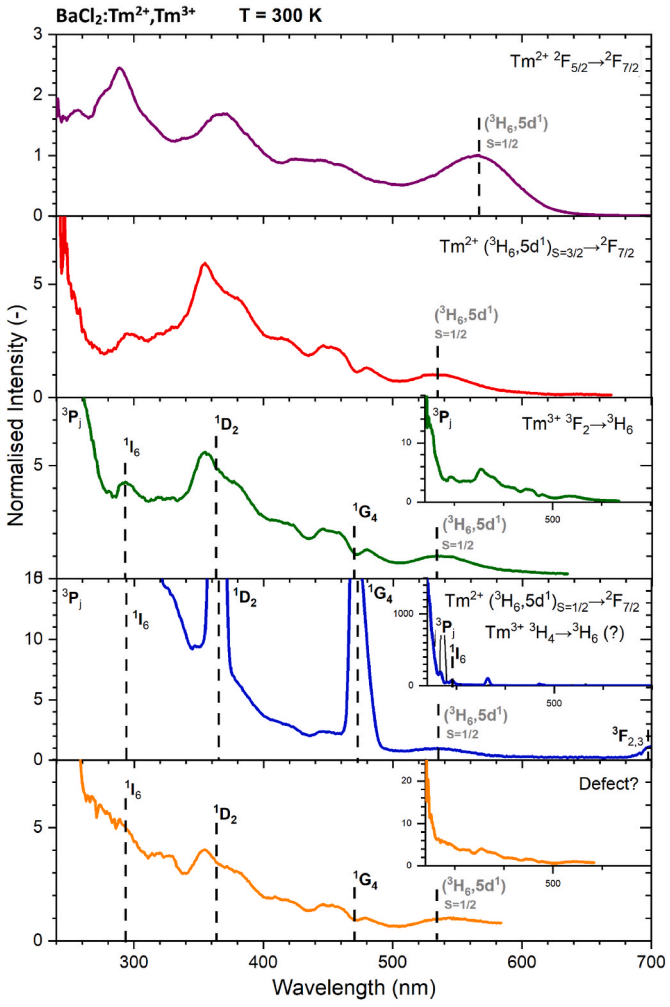

Fig. 4. Normalised room temperature excitation spectra of the $BaCl_2$:Tm^{2+}, Tm^{3+} sample as acquired on the Tm^{2+} $^2F_{5/2} \rightarrow {}^2F_{7/2}$ (purple), $(^3H_6,5\ d^1)_{S\ =\ 1/2} \rightarrow {}^2F_{7/2}$ (red) and $(^3H_6,5\ d^1)_{S\ =\ 3/2} \rightarrow {}^2F_{7/2}$ (blue) emissions and the Tm^{3+} $^3F_2 \rightarrow {}^3H_6$ (green) and possibly $^3H_4 \rightarrow {}^3H_6$ (blue) emissions. Also displayed is an excitation spectrum on the presumed defect emission centred at 610 nm (orange). The purple spectrum was measured with a 1 μm 300 g/mm emission monochromator grating, whereas the other spectra were acquired with a 300 nm 300 g/mm grating; giving rise to a slight wavelength displacement upon comparing the spectra. In the excitation spectrum of the Tm^{3+} $^3F_2 \rightarrow {}^3H_6$ emission (green), signatures of Tm^{3+} excitations are observed; but also the Tm^{2+} $(^3H_6,5\ d^1)_{S\ =\ 1/2}$ and higher energy $4f^{12}5d^1$-levels.

wavelength displacement due to the use of monochromators with different gratings), with a clear depiction of the Tm^{2+} $(^3H_6,5\ d^1)_{S\ =\ 1/2}$ levels and the $4f^{12}5d^1$-levels at higher energy.

The excitation spectrum acquired on the Tm^{3+} $^3F_2 \rightarrow {}^3H_6$ ($4f^{12} \rightarrow 4f^{12}$) emission (green) is highly similar in shape to that obtained for the Tm^{2+} emissions, with weak narrow signature features of the Tm^{3+} $^1G_4$, $^1D_2$, $^1I_6$ and ^3P_j levels present. The clear observation of the Tm^{2+} $(^3H_6,5\ d^1)_{S\ =\ 1/2}$ $4f^{12}5d^1$-levels in the excitation spectrum of Tm^{3+} indicates that these Tm^{2+} levels contribute to and feed the Tm^{3+} $^3F_2 \rightarrow {}^3H_6$ emission, providing further evidence for the $Tm^{2+} \rightarrow Tm^{3+}$ energy transfer. With the Tm^{2+} $(^3H_6,5\ d^1)_{S\ =\ 3/2} \rightarrow {}^2F_{7/2}$ emission located at almost the same wavelength as the Tm^{3+} $^3H_4 \rightarrow {}^3H_6$ emission, the corresponding excitation spectrum (blue) shows clear signs of both the Tm^{2+} $(^3H_6,5\ d^1)_{S\ =\ 1/2}$ and higher energy $4f^{12}5d^1$-levels, as well as the Tm^{3+} $^1G_4$, $^1D_2$, $^1I_6$ and ^3P_j levels. This proves that the Tm^{3+} $^3H_4 \rightarrow {}^3H_6$ emission is definitely present in the red spectrum in Fig. 3, and hidden in the tail of the broad Tm^{2+} $(^3H_6,5\ d^1)_{S\ =\ 3/2} \rightarrow {}^2F_{7/2}$ emission.

The excitation spectrum acquired on the luminescence feature located near 610 nm, portrayed in orange, largely resembles that of the Tm^{2+} $(^3H_6,5\ d^1)_{S\ =\ 3/2} \rightarrow {}^2F_{7/2}$ emission. This shows it being related to Tm^{2+} luminescence, likely coming from Tm^{2+} ions present at or near the surface of the BaCl2:Tm^{2+},Tm^{3+} sample.

3.2.4. *Estimation of the Tm^{2+}-Tm^{3+} distance*

For efficient energy transfer, the average Tm^{2+} and Tm^{3+} ions should be not too far from each other. Assuming a random distribution of Tm^{2+} and Tm^{3+} in the $BaCl_2$ lattice, the average distance R can be estimated using the formula proposed by Blasse [45]:

$$R = 2\left(\frac{3V}{4\pi Zx}\right)^{1/3}$$

In this formula, V is the volume of the unit cell of $BaCl_2$ (V = 359.81 $Å^3$), Z is the number of formula units $BaCl_2$ in a unit cell (Z = 4), and x is the Tm concentration $0 < x < 1$ (corresponding with $0 <$ mol.% < 100 %).

In this way the average Tm^{2+}-Tm^{2+} and Tm^{3+}-Tm^{3+} distances are calculated to be respectively about 39 Å (Tm^{2+}-concentration = 0.3 mol. %) and 28 Å (Tm^{3+}-concentration = 0.8 mol.%), indicating that the average minimum distance between Tm^{2+} and Tm^{3+} is smaller than 28 Å. A somewhat smaller Tm^{2+}-Tm^{3+} distance of about 25 Å results by taking the total (Tm^{2+} + Tm^{3+}) concentration of 1.1 mol.%. So the distance between Tm^{2+} and Tm^{3+} is considerably larger than the critical distances for energy transfer by the multipole-multipole mechanism and in particular the exchange interaction, making the energy transfer from Tm^{2+} to Tm^{3+} quite inefficient for the Tm^{2+}- and Tm^{3+}- concentrations of the studied $BaCl_2$:Tm^{2+},Tm^{3+} sample. The energy transfer efficiency will strongly increase for higher Tm concentrations. For a total (Tm^{2+} + Tm^{3+}) concentration of e.g. 10 mol.% the average distance has dropped to about 12 Å, a reasonable distance for efficient energy transfer by multipole-multipole interaction. Simultaneously, for a constant (Tm^{2+} + Tm^{3+}) concentration, a large Tm^{2+} concentration is favorable for obtaining a high absorption of excitation radiation, while a sufficiently small Tm^{3+} concentration will avoid concentration quenching of the Tm^{3+} emission.

3.3. *Exploring the possibility of $Tm^{2+} \rightarrow Tm^{3+}$ energy transfer in other Tm-doped halides*

As illustrated for the case of Tm-doped orthorhombic $BaCl_2$, the Tm^{2+} $(^3H_6,5\ d^1)_{S\ =\ 1/2} \rightarrow {}^2F_{7/2}$ Spin-Allowed (SA) ($4f^{12}5d^1 \rightarrow 4f^{13}$) emission plays a leading role in the energy transfer to Tm^{3+}, since its energy matches with the energy of the Tm^{3+} $^3H_6 \rightarrow {}^3F_2$, $^3H_6 \rightarrow {}^3F_3$ and $^3H_6 \rightarrow {}^3H_4$ ($4f^{12} \rightarrow 4f^{12}$) transitions. The lower energy of the Tm^{2+} $(^3H_6,5\ d^1)_{S\ =\ 3/2} \rightarrow {}^2F_{7/2}$ Spin-Forbidden (SF) ($4f^{12}5d^1 \rightarrow 4f^{13}$) emission, on the other hand, matches with the energy of the Tm^{3+} $^3H_6 \rightarrow {}^3H_4$ and $^3H_6 \rightarrow {}^3F_3$ ($4f^{12} \rightarrow 4f^{12}$) transitions. However, the energy of both the Tm^{2+} $(^3H_6,5\ d^1)_{S\ =\ 1/2} \rightarrow {}^2F_{7/2}$ SA and $(^3H_6,5\ d^1)_{S\ =\ 3/2} \rightarrow {}^2F_{7/2}$ SF ($4f^{12}5d^1 \rightarrow 4f^{13}$) emissions are host lattice dependent, whereas the energy of the aforementioned Tm^{3+} $^3H_6 \rightarrow {}^3F_{2,3}$, and $^3H_6 \rightarrow {}^3H_4$ ($4f^{12} \rightarrow 4f^{12}$) transitions is, more or less, constant for different halide compounds [42]. Using previously collected data on the energy of the Tm^{2+} $(^3H_6,5\ d^1)_{S\ =\ 1/2} \rightarrow {}^2F_{7/2}$ and $(^3H_6,5\ d^1)_{S\ =\ 3/2} \rightarrow {}^2F_{7/2}$ ($4f^{12}5d^1 \rightarrow 4f^{13}$) emissions, we have explored the option of $Tm^{2+} \rightarrow Tm^{3+}$ energy transfer in Tm-doped halides beyond $BaCl_2$ [27–30,37].

In Fig. 5, the lower part shows the peak energy of the broad Tm^{2+} $(^3H_6,5\ d^1)_{S\ =\ 1/2} \rightarrow {}^2F_{7/2}$ and $(^3H_6,5\ d^1)_{S\ =\ 3/2} \rightarrow {}^2F_{7/2}$ ($4f^{12}5d^1 \rightarrow 4f^{13}$) emissions (symbols) and their full energy range (+ and -, coloured strokes) with FWHM indicated (X and ✱); all for different Tm-doped halides. The upper part in Fig. 5 provides the complementary energies of the Tm^{2+} $(^3H_6,5\ d^1)_{S\ =\ 1/2}$ and $(^3H_6,5\ d^1)_{S\ =\ 3/2}$ ($4f^{12}5d^1$) excitation levels (symbols), including the minimal energy from which $4f^{13} \rightarrow 4f^{12}5d^1$ excitations occur (-, coloured strokes). The excitation energies of the Tm^{3+} $^3H_6 \rightarrow {}^3F_2$, $^3H_6 \rightarrow {}^3F_3$ and $^3H_6 \rightarrow {}^3H_4$ ($4f^{12} \rightarrow 4f^{12}$)

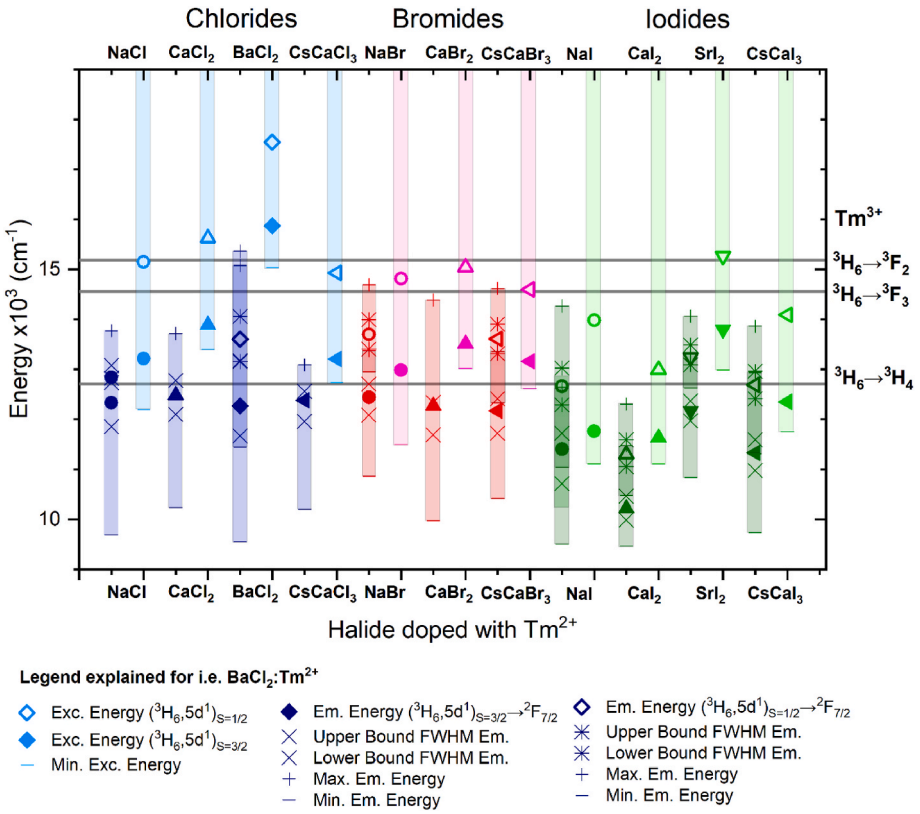

Fig. 5. Diagram showing the excitation energy of the Tm^{3+} $^3H_6 \rightarrow {}^3F_2$, $^3H_6 \rightarrow {}^3F_3$ and $^3H_6 \rightarrow {}^3H_4$ transitions (solid black lines), the energy range of the Tm^{2+} $4f^{12}5d^1$ excitation levels (light colours) with the peak energies of the $(^3H_6,5\ d^1)_{S\ =\ 1/2}$ (open symbols) and $(^3H_6,5\ d^1)_{S\ =\ 3/2}$ (closed symbols) levels marked, and the emission energies of the Tm^{2+} $4f^{12}5d^1 \rightarrow 4f^{13}$ emissions (dark colours) with the broad $(^3H_6,5\ d^1)_{S\ =\ 1/2} \rightarrow {}^2F_{7/2}$ (open symbols) and $(^3H_6,5\ d^1)_{S\ =\ 3/2} \rightarrow {}^2F_{7/2}$ (closed symbols) emission displayed over their full energy range and FWHM indicated; all for known Tm-doped chlorides (blueish), bromides (reddish) and iodides (greenish) [27–30, 37].

Note 1: For NaCl:Tm^{2+}, two $(^3H_6,5\ d^1)_{S\ =\ 3/2} \rightarrow {}^2F_{7/2}$ emission peaks were previously found, which are most likely related to two different Tm^{2+} centres due to the necessity of charge compensation effects as Tm^{2+} enters the Na^+-site [27].

Note 2: Absence of Tm^{2+} $(^3H_6,5\ d^1)_{S\ =\ 1/2} \rightarrow {}^2F_{7/2}$ emission (open symbols) in NaCl:Tm^{2+}, $CaCl_2$:Tm^{2+},$CsCaCl_3$:Tm^{2+}, $CaBr_2$:Tm^{2+}.

transitions are added as horizontal black lines. A quantification of the data is provided in Table S1 in section 9.2 of the SI, including a ratio between the peak intensities of the Tm^{2+} $(^3H_6,5\ d^1)_{S\ =\ 3/2} \rightarrow {}^2F_{7/2}$ and $(^3H_6,5\ d^1)_{S\ =\ 1/2} \rightarrow {}^2F_{7/2}$ ($4f^{12}5d^1 \rightarrow 4f^{13}$) emissions after excitation into the Tm^{2+} $(^3H_6,5\ d^1)_{S\ =\ 1/2}$ $4f^{12}5d^1$-levels at 20 K.

As Fig. 5 shows, only for $BaCl_2$:Tm^{2+},Tm^{3+} there is a sizeable overlap in energy between the Tm^{2+} $(^3H_6,5\ d^1)_{S\ =\ 1/2} \rightarrow {}^2F_{7/2}$ SA emission (open blue diamond) and the Tm^{3+} $^3H_6 \rightarrow {}^3F_3$ and $^3H_6 \rightarrow {}^3H_4$ transitions (middle and lower black lines); enabling $Tm^{2+} \rightarrow Tm^{3+}$ energy transfer. In addition, there is even a small overlap in energy with the Tm^{3+} $^3H_6 \rightarrow {}^3F_2$ transition (upper black line). For $CsCaBr_3$:Tm^{2+},Tm^{3+} and NaBr:Tm^{2+}, Tm^{3+}; the Tm^{2+} $(^3H_6,5\ d^1)_{S\ =\ 1/2} \rightarrow {}^2F_{7/2}$ SA emission shares a small overlap with the Tm^{3+} $^3H_6 \rightarrow {}^3F_3$ transition. In case of $CsCaBr_3$:Tm^{2+}, Tm^{3+} the aforementioned Tm^{2+} emission also shares a small overlap with the Tm^{3+} $^3H_6 \rightarrow {}^3H_4$ transition. However, as can be perceived from Fig. 5, the energy of the Tm^{2+} $(^3H_6,5\ d^1)_{S\ =\ 1/2} \rightarrow {}^2F_{7/2}$ SA emission of both compounds has a much stronger overlap with the energy of the Tm^{2+} $^2F_{7/2} \rightarrow (^3H_6,5\ d^1)_{S\ =\ 3/2}$ excitation transitions, resulting in a strong non-radiative energy transfer from the Tm^{2+} $(^3H_6,5\ d^1)_{S\ =\ 1/2}$ level to Tm^{2+} $(^3H_6,5\ d^1)_{S\ =\ 3/2}$ level, as described in our previous study [37]. This strong process explains why the intensity of the Tm^{2+} $(^3H_6,5\ d^1)_{S\ =\ 1/2} \rightarrow {}^2F_{7/2}$ SA emission is weak in both compounds and weak or absent in other Tm-doped halides. The absence of this process in orthorhombic $BaCl_2$:Tm^{2+} results in strong Tm^{2+} $(^3H_6,5\ d^1)_{S\ =\ 1/2} \rightarrow {}^2F_{7/2}$ SA emission. We therefore suspect that the $Tm^{2+} \rightarrow Tm^{3+}$ energy transfer in Tm-doped $CsCaBr_3$ and NaBr, via the Tm^{2+} $(^3H_6,5\ d^1)_{S\ =\ 1/2} \rightarrow {}^2F_{7/2}$ SA emission, will only be very weakly observed.

For $BaCl_2$:Tm^{2+},Tm^{3+}; the energy of the Tm^{2+} $(^3H_6,5\ d^1)_{S\ =\ 3/2} \rightarrow {}^2F_{7/2}$ SF emission (blue diamond) overlaps with the Tm^{3+} $^3H_6 \rightarrow {}^3F_3$ and $^3H_6 \rightarrow {}^3H_4$ transitions (middle and lower black lines); allowing for $Tm^{2+} \rightarrow Tm^{3+}$ energy transfer. For Tm-doped NaCl, NaBr, $CaCl_2$ $CaBr_2$, SrI_2, $CsCaCl_3$, $CsCaBr_3$ and $CsCaI_3$; the Tm^{2+} $(^3H_6,5\ d^1)_{S\ =\ 3/2} \rightarrow {}^2F_{7/2}$ SF emission also overlaps with the Tm^{3+} $^3H_6 \rightarrow {}^3H_4$ transition. In case of Tm-doped NaCl, NaBr and $CaCl_2$; the overlap occurs within the FWHM of the Tm^{2+} $(^3H_6,5\ d^1)_{S\ =\ 3/2} \rightarrow {}^2F_{7/2}$ SF emission peak, making it likely to encounter relatively strong signatures of $Tm^{2+} \rightarrow Tm^{3+}$ energy transfer. The $Tm^{2+} \rightarrow Tm^{3+}$ energy transfer in these compounds would, however, be competing with thermal quenching of the Tm^{2+} $(^3H_6,5\ d^1)_{S\ =\ 3/2} \rightarrow {}^2F_{7/2}$ SF emission [27,29].

These processes will be much weaker at low temperatures. The $Tm^{2+} \rightarrow Tm^{3+}$ energy transfer in the aforementioned compounds would manifest itself via the appearance of the Tm^{3+} $^3H_4 \rightarrow {}^3H_6$ emission. However, at low temperatures, the sharp Tm^{3+} $^3H_4 \rightarrow {}^3H_6$ ($4f^{12} \rightarrow 4f^{12}$) emission peak would be positioned on top of the broad Tm^{2+} $(^3H_6,5\ d^1)_{S\ =\ 3/2} \rightarrow {}^2F_{7/2}$ SF ($4f^{12}5d^1 \rightarrow 4f^{13}$) emission, making it difficult to separate between the two.

Summarizing, conditions for efficient $Tm^{2+} \rightarrow Tm^{3+}$ energy transfer are strong overlap of the Tm^{2+} $(^3H_6,5\ d^1)_{S\ =\ 1/2} \rightarrow {}^2F_{7/2}$ SA ($4f^{12}5d^1 \rightarrow 4f^{13}$) emission with the Tm^{3+} $^3H_6 \rightarrow {}^3F_3$ or $^3H_6 \rightarrow {}^3H_4$ ($4f^{12} \rightarrow 4f^{12}$) transitions, or of the Tm^{2+} $(^3H_6,5\ d^1)_{S\ =\ 3/2} \rightarrow {}^2F_{7/2}$ SF ($4f^{12}5d^1 \rightarrow 4f^{13}$) emission with the Tm^{3+} $^3H_6 \rightarrow {}^3H_4$ ($4f^{12} \rightarrow 4f^{12}$) transition; while the Tm^{2+} $(^3H_6,5\ d^1)_{S\ =\ 1/2} \rightarrow {}^2F_{7/2}$ SA emission should not overlap with the Tm^{2+} $(^3H_6,5\ d^1)_{S\ =\ 3/2}$ $4f^{12}5d^1$ excitation levels.

3.4. Practical use of Tm^{2+}→Tm^{3+} energy transfer

The Tm^{2+}→Tm^{3+} energy transfer in Tm-doped halides, as demonstrated for orthorhombic $BaCl_2$:Tm^{2+},Tm^{3+}, may be useful in various opto-electronic devices. For example, the Tm^{2+}→Tm^{3+}energy transfer can add special features to Tm^{2+}/Tm^{3+}-co-doped phosphors that are being used in high-sensitivity optical thermometers. Moreover, it can also be used in high-sensitivity optical thermometers that are based on the luminescence of divalent and trivalent thulium ions in $CaAl_4O_7$:$Tm^{2+/3+}$ that operate in cryogenic and high temperature ranges [36]. In such a device, the thermal evolution of the Tm^{3+} $^3F_{2,3}$ → $^3H_6$ and $^3H_4$→$^3H_6$ luminescence can be remotely monitored to establish the surrounding temperature.

In addition, the Tm^{2+}→Tm^{3+}energy transfer can be used in the design optimization of spectral conversion layers, such as Luminescence Solar Concentrators (LSCs). LSC devices ideally absorb sunlight over a broad wavelength range, to subsequently emit light of a different wavelength that is optically guided towards a solar cell [26,46,47]. An LSC device based on the Tm^{2+}→Tm^{3+} energy transfer in Tm-doped halides, could focus the Tm^{3+} $^3F_{2,3}$ → $^3H_6$ and $^3H_4$→$^3H_6$ luminescence, with respective energies of 1.76 and 1.54 eV, onto $MASn(BrI)_3$ perovskite solar cells with bandgap energies ranging from 1.30 to 2.15 eV [48]. Previous research by Ten Kate et al. [26] has shown that Tm^{2+} as doped in halides are able to absorb a vast percentage of the AM1.5 solar spectrum. Although halides are hygroscopic, glass-glass lamination techniques [49] and the incorporation of fluorine [50], creating halide solid solutions, would protect the material against degradation. Similar hydrolysis-sensitive materials such as $LaBr_3$:Ce^{3+} are successfully used in commercial scintillator applications for harsh environmental conditions by encapsulating it in an aluminium housing with fused silica optical window.

4. Summary and conclusions

In this study, we have demonstrated for the very first time Tm^{2+}→Tm^{3+} energy transfer. It was found to occur in orthorhombic $BaCl_2$:Tm^{2+},Tm^{3+} with the cotunnite structure. Tm^{2+} $^2F_{7/2}$→($^3H_6$,5 d^1)$_{S = 1/2}$ ($4f^{13}$→$4f^{12}5d^1$) photoexcitation leads to relatively strong ($^3H_6$,5 d^1)$_{S = 1/2}$ → $^2F_{7/2}$ SA ($4f^{12}5d^1$→$4f^{13}$) luminescence with subsequent energy transfer to nearby Tm^{3+} ions triggering $^3H_6$→$^3F_{2,3}$ and $^3H_6$→$^3H_4$ ($4f^{12}$→$4f^{12}$) excitation and resulting in Tm^{3+} $^3F_{2,3}$ → $^3H_6$ and $^3H_4$→$^3H_6$ ($4f^{12}$→$4f^{12}$) luminescence. In addition, Tm^{2+} ($^3H_6$,5 d^1)$_{S = 1/2}$→($^3H_6$,5 d^1)$_{S = 3/2}$ ($4f^{12}5d^1$→$4f^{12}5d^1$) multiphonon relaxation leads to Tm^{2+} ($^3H_6$,5 d^1)$_{S = 3/2}$ → $^2F_{7/2}$ SF ($4f^{12}5d^1$→$4f^{13}$) luminescence, with energy being transferred to Tm^{3+} ions at close distance leading to $^3H_6$→$^3F_3$ and $^3H_6$→$^3H_4$ ($4f^{12}$→$4f^{12}$) excitation, followed by Tm^{3+} $^3F_3$→$^3H_6$ and $^3H_4$→$^3H_6$ ($4f^{12}$→$4f^{12}$) luminescence.

However, an overlap of the Tm^{2+} ($^3H_6$,5 d^1)$_{S = 1/2}$ → $^2F_{7/2}$ SA ($4f^{12}5d^1$→$4f^{13}$) emission with the Tm^{2+} $^2F_{7/2}$→($^3H_6$,5 d^1)$_{S = 3/2}$ ($4f^{13}$→$4f^{12}5d^1$) excitation, will result in strong non-radiative energy transfer from the ($^3H_6$,5 d^1)$_{S = 1/2}$ level to ($^3H_6$,5 d^1)$_{S = 3/2}$ level, competing with the aforementioned Tm^{2+}→Tm^{3+} energy transfer. $BaCl_2$:Tm^{2+},Tm^{3+} is the only Tm-doped halide found so far for which there is a negligible overlap between Tm^{2+} ($^3H_6$,5 d^1)$_{S = 1/2}$ → $^2F_{7/2}$ SA emission and Tm^{2+} $^2F_{7/2}$→($^3H_6$,5 d^1)$_{S = 3/2}$ excitation, enabling the possibility for efficient Tm^{2+}→Tm^{3+} energy transfer. Despite this, we do expect to see Tm^{2+}→Tm^{3+} energy transfer based on the Tm^{2+} ($^3H_6$,5 d^1)$_{S = 3/2}$ → $^2F_{7/2}$ SF emission in Tm-doped NaX, CaX_2, $CsCaX_3$ (X = Cl, Br), $CsCaI_3$ and SrI_2. It would be most strongly present in Tm-doped NaCl, NaBr and $CaCl_2$; to be confirmed by a clear observation of the Tm^{3+} $^3H_4$→$^3H_6$ ($4f^{12}$→$4f^{12}$) emission on top of the broad Tm^{2+} ($^3H_6$,5 d^1)$_{S = 3/2}$ → $^2F_{7/2}$ SF ($4f^{12}5d^1$→$4f^{13}$) emission band.

The Tm^{2+}→Tm^{3+} energy transfer, demonstrated in this work for $BaCl_2$:Tm^{2+},Tm^{3+} and possibly also present in some other halide compounds, competes with: the thermal quenching of the Tm^{2+} ($^3H_6$,5 d^1)$_{S = 1/2}$ → $^2F_{7/2}$ and ($^3H_6$,5 d^1)$_{S = 3/2}$ → $^2F_{7/2}$ emissions via ($^3H_6$,5 d^1)$_{S = 1/2}$ → $^2F_{5/2}$ and ($^3H_6$,5 d^1)$_{S = 3/2}$ → $^2F_{5/2}$ ($4f^{12}5d^1$→$4f^{13}$) interband crossing, and thermal quenching via the conduction band. In order to minimize the quenching effects, competing with the Tm^{2+}→Tm^{3+} energy transfer, additional research is needed into the engineering of the Tm^{2+} $4f^{12}5d^1$ energy levels via for instance halide solid solutions. In addition, time-resolved spectroscopy measurements should be performed to gather more insights into the mechanism and efficiency of the Tm^{2+}→Tm^{3+} energy transfer as well as and research on optimization of the interatomic distances between the Tm^{2+} and Tm^{3+} ions, via a finetuning of the Tm^{2+} and Tm^{3+} doping concentrations.

The discovered Tm^{2+}→Tm^{3+} energy transfer that takes place in Tm-doped halides may be useful in high-sensitivity optical thermometers and in the design of spectral conversion layers, such as luminescence solar concentrators.

CRediT authorship contribution statement

M.P. Plokker: Writing – review & editing, Writing – original draft, Visualization, Validation, Supervision, Software, Resources, Project administration, Methodology, Investigation, Formal analysis, Data curation, Conceptualization. **S.W. Bergkamp:** Visualization, Validation, Software, Investigation, Formal analysis, Conceptualization. **H.T. Hintzen:** Writing – review & editing, Writing – original draft, Supervision, Methodology, Investigation, Formal analysis, Conceptualization.

Declaration of competing interest

The authors declare that they have no known competing financial interests or personal relationships that could have appeared to influence the work reported in this paper.

Acknowledgement

The authors would like to thank J.T.M. de Haas (TU Delft) for experimental support with the luminescence measurements.

Appendix A. Supplementary data

Supplementary data to this article can be found online at https://doi.org/10.1016/j.omx.2025.100432.

Data availability

Data will be made available on request.

References

[1] M. Suta, C. Wickleder, Synthesis, spectroscopic properties and applications of divalent lanthanides apart from Eu^{2+}, J. Lumin. 210 (2019) 210–238.
[2] J.-C.G. Bunzli, V.K. Pecharsky, Handbook on the Physics and Chemistry of Rare Earths, Chapter 293, expanding the + 2 oxidation state of the rare-earth metals. Uranium, and Thorium in Molecular Complexes, 2016, ISBN 978-0-444-63699-7.
[3] F. Wang, H. Chen, S. Zhang, S. Zhang, H. Jin, Energy transfer of Eu^{2+}→Eu^{3+} improves the photoluminescence properties of orange-red phosphor La2O2S:Eu, J. Alloys Compd. 969 (2023) 172394.
[4] W. Chen, Y. Ouyang, M. Mo, H. Zhang, O. Su, Observation of energy transfer from Eu^{2+} to Eu^{3+} and tunable luminescence in phosphors YF_3:Eu prepared by hydrothermal method, J. Lumin. 229 (2021) 117672.
[5] S. Li, L. Wang, D. Tang, Y. Cho, X. Liu, X. Zhou, L. Lu, L. Zhang, T. Takeda, N. Hirosaki, R.-J. Xie, Achieving high quantum efficiency narrow-band β-Sialon: Eu^{2+} phosphors for high-brightness LCD backlights by reducing the Eu^{3+} luminescence killer, Chem. Mater. 30 (2018) 494–505.
[6] C. van Aarle, R. Ingham, C. van der Heijden, K. Budwilowitz, M. Niehe, I. Dugulan, H.T. Hintzen, Demonstration of Eu^{3+} → Eu^{2+} energy transfer in NIR emitting CaO: Eu^{2+},Eu^{3+} LED phosphor and its implication for the role of Eu^{3+} as a killer center for long wavelength Eu^{2+} emission, Adv. Opt. Mater. 12 (35) (2024) 2401738.
[7] W. Chen, Y. Ouyang, M. Mo, H. Zhang, Q. Su, Observation of energy transfer from Eu^{2+} to Eu^{3+} and tunable luminescence in phosphors YF_3:Eu prepared by hydrothermal method, J. Lumin. 229 (2021) 117672.
[8] W.B. Dai, Mechanism of the reduction and energy transfer between Eu^{2+} and Eu^{3+} in Eu-doped $CaAl_2Si_2O_8$ materials prepared in air, J. Mater. Chem. C. 2 (2014) 3952.

[9] X. Gao, H. Liu, X. Yang, Y. Tian, X. Lua, L. Han, A novel Eu^{3+}/Eu^{2+} co-doped $MgSrLa_8(SiO_4)_6O_2$ single-phase white light phosphor for white LEDs, RSC Adv. 7 (2017) 1711.

[10] R. Yu, J. Wang, Z. Zhao, M. Li, S. Huo, J. Li, J. Wang, Luminescence property and energy transfer behavior of apatite-type $Ca_4La_6(SiO_4)_4(PO_4)_2O_2$:$Tb^{3+}$, Eu^{3+} phosphor, Mater. Lett. 160 (2015) 294.

[11] Z. Wang, H. Fu, X. Zhan, B. Tong, G. Ma, H.T. Hintzen, Photoluminescence and ratiometric thermo-response of Eu^{2+} and Eu^{3+} in $BaAl_2B_2O_7$:Eu^{2+},Eu^{3+} phosphor materials, J. Rare Earths 42 (2023).

[12] N.B. Aranda, R.F. Muniz, M.L. Baesso, A.C. Bento, H.M.S. Deroide, A.N. Medina, L. A.O. Nunes, J.R. Silva, S.M. Lima, L.H.C. Andrade, J.H. Rohling, Downconversion luminescence in Ce^{3+}, Yb^{2+}, and Yb^{3+} co-doped low silica calcium aluminosilicate glasses: potential for spectral conversion in solar cell technology, Opt. Mater. 142 (2023).

[13] M. Yamaga, S.I. Tsuda, J.P.R. Wells, T.P.J. Han, Dynamics processes between Sm2 +, Sm3+ and color centers in KY3F10 : sm crystals, JCPR 15 (3) (2014) 167–172.

[14] Z.J. Kiss, Energy levels of divalent thulium in CaF_2, Phys. Rev. 127 (3) (1962) 718–724.

[15] D.S. McClure, Z. Kiss, Survey of the spectra of the divalent rare-earth ions in cubic crystals, J. Chem. Phys. 39 (12) (1963) 3251–3257.

[16] R.C. Duncan Jr., Z.J. Kiss, Continuously operating CaF_2:Tm^{2+} optical maser, Appl. Phys. 3 (2) (1963) 23–24.

[17] Z.J. Kiss, R.J. Pressley, Crystalline solid lasers, Appl. Opt. 5 (10) (1966) 1474–1486.

[18] O.S. Wenger, C. Wickleder, K.W. Krämer, H.U. Güdel, Upconversion in a divalent rare earth ion: optical absorption and luminescence spectroscopy of Tm^{2+} doped $SrCl_2$, J. Lumin. 94–95 (2001) 101–105.

[19] J. Grimm, E. Beurer, H.U. Güdel, Crystal absorption spectra in the region of 4f-4f and 4f-5d excitations in Tm^{2+}-doped $CsCaCl_3$, $CsCaBr_3$, and $CsCaI_3$, Inorg. Chem. 45 (2006) 10905–10908.

[20] J. Grimm, H.U. Güdel, Five different types of spontaneous emission simultaneously observed in Tm^{2+} doped $CsCaBr_3$, Chem. Phys. Lett. 404 (2005) 40–43.

[21] E. Beurer, J. Grimm, P. Gerner, H.U. Güdel, New type of near-infrared to visible photon upconversion in Tm^{2+}-doped $CsCaI_3$, J. Am. Chem. Soc. 128 (2006) 3110–3111.

[22] E. Beurer, J. Grimm, P. Gerner, H.U. Güdel, Absorption, light emission, and upconversion properties of Tm^{2+}-doped $CsCaI_3$ and $RbCaI_3$, Inorg. Chem. 45 (2006) 9901–9906.

[23] J. Grimm, J.F. Suyver, E. Beurer, G. Carver, H.U. Güdel, Light-emission and excited-state dynamics in Tm^{2+} doped $CsCaCl_3$, $CsCaBr_3$, and $CsCaI_3$, J. Phys. Chem. B 110 (2006) 2093–2101.

[24] J. Grimm, O.S. Wenger, K.W. Krämer, H.U. Güdel, 4f–4f and 4f–5d excited states and luminescence properties of Tm^{2+}-doped CaF_2, $CaCl_2$, $SrCl_2$ and $BaCl_2$, J. Lumin. 126 (2007) 590–596.

[25] J. Grimm, E. Beurer, P. Gerner, H.U. Güdel, Upconversion between 4f–5d excited states in Tm^{2+}-doped $CsCaCl_3$, $CsCaBr_3$, and $CsCaI_3$, Eur. J. Chem. 13 (2007) 1152–1157.

[26] O.M. ten Kate, K.W. Krämer, E. Van der Kolk, Efficient luminescent solar concentrators based on self-absorption free Tm^{2+} doped halides, Sol. Energy Mater. Sol. Cells 140 (2015) 115–120.

[27] M.P. Plokker, E. van der Kolk, Temperature dependent relaxation dynamics of luminescent NaX:Tm^{2+} (X=Cl, Br, I), J. Lumin. 216 (2019) 116694.

[28] M.P. Plokker, W. Hoogsteen, R.D. Abellon, K.W. Krämer, E. van der Kolk, Concentration and temperature dependent luminescence properties of the SrI2-TmI2 system, J. Lumin. 225 (2020) 117327.

[29] M.P. Plokker, I.C. van der Knijff, A.V. de Wit, B. Voet, T. Woudstra, V. Khanin, P. Dorenbos, E. van der Kolk, Experimental and numerical analysis of Tm^{2+} excited-states dynamics and luminescence in CaX_2 (X = Cl, Br, I), J. Phys. Condens. Matter 33 (25) (2021) 255701.

[30] M.P. Plokker, D.A. Biner, N. Dusoswa, P. Dorenbos, K.W. Krämer, E. van der Kolk, Photoluminescence and excited states dynamics of Tm^{2+}-doped $CsCa(Cl/Br)_3$ and $CsCa(Br/I)_3$ perovskites, J. Phys. Mater. 4 (4) (2021) 045004.

[31] Z. Cao, X. Wei, L. Zhao, T. Chen, M. Yin, Investigation of SrB_4O_7:Sm^{2+} as a multimode temperature sensor with high sensitivity, ACS Appl. Mater. Interfaces 8 (50) (2016). P.34546–3455.

[32] P. Solarz, J. Komar, M. Głowacki, M. Berkowski, W. Ryba-Romanowski, Spectroscopic characterization of SrB_4O_7:Tm^{2+}, a potential laser material and optical temperature sensor, RSC Adv. 7 (2017) 21085–21092.

[33] M. Karbowiak, R. Lisiecki, P. Solarz, J. Komar, W. Ryba-Romanowski, Spectroscopic peculiarities of CsCaI3:Tm2+ single crystals examined through one-photon and excited state excitation spectroscopy, J. Alloys Compd. 1165–1171 (2018) 740.

[34] T. Zheng, M. Sójka, M. Runowski, P. Woźny, S. Lis, E. Zych, Tm^{2+} activated SrB_4O_7 bifunctional sensor of temperature and pressure—highly sensitive, multi-parameter luminescence thermometry and manometry, Adv. Opt. Mater. 9 (22) (2021) 34546–34551.

[35] Q. Zhang, Z. Liao, L. Qiu, X. Wei, Y. Chen, M. Yin, Investigation of SrB_4O_7:Tm^{2+} luminescence for temperature imaging with high sensitivity based on time-resolved luminescence, Dalton Trans. 53 (2024) 14289–14299.

[36] R. Panda, M. Behera, M. Hegde, R. Arun Kumar, G. Venugopal, P. Wozny, K. Soler-Carracedo, M. Runowski, High-sensitivity optical thermometer based on the luminescence of divalent and trivalent thulium ions in $CaAl_4O_7$:$Tm^{2+/3+}$ operating in cryogenic and high temperature ranges, J. Mater. Chem. C 13 (2025) 8776–8791.

[37] M.P. Plokker, S. Vlaar, A.H.J. Bakx, E. van der Kolk, P. Dorenbos, H.T. Hintzen, Evaluating the Tm^{2+} $4f^{12}5d^1 \rightarrow 4f^{13}$ and $4f^{13} \rightarrow 4f^{13}$ luminescence and quenching dynamics in orthorhombic $BaCl_2$, J. Phys. Chem. 127 (38) (2023) 19017–19026.

[38] M.P. Plokker, H.T. Hintzen, The influence of the conduction band of $BaCl_2$ on the thermal quenching of the Tm^{2+} $4f^{12}5d^1 \rightarrow 4f^{13}$ and $4f^{13} \rightarrow 4f^{13}$ luminescence in orthorhombic $BaCl_2$:$Tm^{2+/3+}$, Opt. Mater. X 25 (2025).

[39] L.H. Brixner, A. Ferretti, Eu^{2+} fluorescence in $BaCl_2$, J. Solid State Chem. 18 (1976) 111–116.

[40] E. Rogers, P. Dorenbos, J.T.M. de Haas, E. van der Kolk, Experimental study of the $4f^n \rightarrow 4f^n$ and $4f^n \rightarrow 4f^{n-1}$ $5d^1$ transitions of the lanthanide diiodides LnI_2 (Ln = Nd, Sm, Eu, Dy, Tm, Yb), J. Phys. Condens. Matter 24 (27) (2012).

[41] W.T. Carnall, G.L. Goodman, K. Rajnak, R.S. Rana, A systematic analysis of the spectra of the lanthanide doped into single crystal LaF_3, J. Mater. Chem. 90 (Nr. 7) (1989) 3443.

[42] G.H. Dieke, H.M. Crosswhite, The spectra of the doubly and triply ionized rare earths, Appl. Opt. 2 (Iss. 7) (1963) 675–686.

[43] B.M. Gareev, A.M. Abdrakhmanov, S.M. Yakupova, G.L. Sharipov, Single-bubble sonoluminescence of itterbium(II or III) and thulium(II or III) chloride nanoparticles colloidal suspensions in dodecane, Colloids Surf., A Physicochem. Eng. Asp. 700 (Nr) (2024) 134770.

[44] H.V. Lauer, F.K. Fong, Role of the $4f^n5d$ band in the radiationless $^5D_1 \rightarrow {}^5D_0$ coupling in $BaCl_2$:Sm^{2+} and $BaBr_2$:Sm^{2+}, J. Chem. Phys. 65 (1976).

[45] G. Blasse, Energy transfer in oxidic phosphors, Philips Res. Rep. 24 (1969) 131–144.

[46] M.G. Debije, P.P.C. Verbunt, Thirty years of luminescent solar concentrator research: solar energy for the built environment, Adv. Energy Mater. 2 (2011).

[47] F. Meinardi, F. Bruni, S. Brovelli, Luminescent solar concentrators for building-integrated photovoltaics, Nat. Rev. Mater. 2 (17072) (2017).

[48] M. Helal Miah, M. Uddin Khandaker, B. Rahman, M. Nur-E-Alamde, M. Aminul Islam, Band gap tuning of perovskite solar cells for enhancing the efficiency and stability: issues and prospects, RSC Adv. 14 (2024) 15876–15906.

[49] G. Cattaneo, A. Faes, H.-Y. Li, F. Galliano, M. Gragert, Y. Yao, R. Grischke, T. Söderström, M. Despeisse, C. Ballif, L.E. Perret-Aebi, Lamination process and encapsulation materials for glass–glass PV module design, Photovoltaics Int. 82 (2015).

[50] M. Zhuravleva, L. Stand, H. Wei, C. Hobbs, L.A. Boatner, J.O. Ramey, K. Shah, A. Burger, E. Rowe, P. Bhattacharya, E. Tupitsyn, C.L. Melcher, Hygroscopicity evaluation of halide scintillators, in: Conference: Nuclear Science Symposium and Medical Imaging Conference (NSS/MIC), IEEE, Seoul, South Korea, 2013.